Journal of Histochemistry & Cytochemistry 59(6) 639–648

DOI: 10.1369/0022155411408315
http://jhc.sagepub.com
SAGE

The Open Microcirculation in Human Spleens: A Three-Dimensional Approach

Birte Steiniger, Michael Bette, and Hans Schwarzbach
Institute of Anatomy and Cell Biology (BS,MB) and Faculty of Mathematics and Computer Science (HS), University of Marburg, Marburg, Germany.

Summary

It has long been debated whether the red pulp of human spleens harbors an open or a closed microcirculation or both. To solve this issue, the authors differentially stained the endothelium in red pulp arterial microvessels and in venous sinuses using brightfield and fluorescence immunohistology with reagents against CD34 and CD141. Three-dimensional models of red pulp arterial microvessels and sinuses were derived from serial double-stained paraffin sections with the help of license-free open-access software. In each model, arterial microvascular ends were traced and verified by reference to the original serial sections. In total, 142 ends were analyzed in the specimens of three individuals. None of these ends was connected to a sinus, suggesting that the human splenic red pulp harbors an entirely open circulatory system. Thus, the spleen is the only human organ where blood passes through spaces not lined by endothelia or other barrier-forming cells. (J Histochem Cytochem 59:639-648, 2011)

Keywords

human spleen, open circulation, 3-D reconstruction, CD34, CD141

The spleen represents the only human organ with a largely unknown microcirculation. This is due to two unique aspects of splenic red pulp vasculature, which deviate from the standard pattern of arterioles, capillaries, and venules found in most other organs: First, the splenic red pulp harbors a specialized type of microvessel, the sinuses. These sinuses have gaps between their endothelial lining cells and hoop-like rudiments of a basement membrane permitting red and white blood cells to enter from the outside (Fujita 1974; Fujita et al. 1985). Sinuses form the initial part of the venous microcirculation and continue into venules, which successively form larger veins. In contrast to other organs, splenic sinuses do not represent the equivalents of capillaries, but they clearly exist in addition to capillaries. Second, the splenic cords, which together with the sinuses form the splenic red pulp, contain large numbers of red and white blood cells in open spaces not lined by endothelial cells (Steiniger and Barth 2000). These spaces are delimited by fibroblasts ensheathing collagenous fibers and other components of the extracellular matrix. The splenic cords thus comprise the stromal framework of an open circulation. In addition, they harbor a meshwork of arterioles and capillaries containing endothelial cells. Whether these vessels are directly connected to sinuses is controversial in humans.

The facts mentioned above are consistent with three alternative arrangements of the red pulp microvasculature. First, certain red pulp capillaries might join the sinuses and form a closed system in addition to an open system where other capillaries empty blood into the cord spaces. This blood would return into the sinuses from the outside. Second, besides the open circulation, a closed system consisting of red pulp capillaries that continue directly into venules instead of sinuses might exist. Third, there might be

Received for publication October 10, 2010; accepted March 22, 2011

Corresponding Author:
Birte Steiniger, Institute of Anatomy and Cell Biology, University of Marburg, Robert-Koch-Str. 8, D-35032 Marburg, Germany.
E-mail: steinigb@staff.uni-marburg.de

Supplementary material for this article is available on the *Journal of Histochemistry & Cytochemistry* Web site at http://jhc.sagepub.com/supplemental.

an exclusively open microcirculation system without any connections of capillaries to sinuses and/or venules.

To solve the issue, we performed three-dimensional (3-D) reconstructions of 14 to 30 serial sections of red pulp tissue double-stained for CD34 and CD141 (thrombomodulin) in three individuals using two different immunohistological techniques. CD34 and CD141 are primarily expressed in arteriolar/capillary endothelia and in sinus endothelia, respectively (Steiniger et al. 2007). In addition, we intended to establish a method for future studies enabling the construction of a 3-D-model at a millimeter scale for visualizing the microvasculature of entire splenic follicles based on color information. Such a method appears extremely laborious, because in contrast to visualization methods that directly yield 3-D information, such as computed tomography, magnetic resonance tomography, or confocal microscopy, the third dimension has to be reconstructed from hundreds of serial sections. The method is associated with xy resolution at a micrometer scale but has a lower resolution in the z direction, which is, however, not relevant at the dimension indicated.

To demonstrate the feasibility of the method, we present 3-D reconstructions of the human red pulp microvasculature derived from a small number of serial sections and show that high equipment costs or undue time expenditure can be avoided. We found a rather large number of ends in cord microvessels, and these ends did not anastomose with sinuses or venules. In single sections, certain ends exhibited a funnel-shaped complex morphology. In summary, the data strongly suggest that the splenic red pulp microcirculation forms an entirely open system in humans.

Materials and Methods

Specimens

Spleen specimens were derived from healthy organ donors (specimens 1 and 2 from a 22-year-old man, specimens 3 and 4 from a 15-year-old male, specimens 5 and 6 from a 50-year-old woman) in accordance with the regulations of the local ethics committee. The specimens were fixed in 3.7% aqueous formalin for 24 hr, dehydrated, and embedded in paraffin.

Immunohistology

Fourteen to 30 serial sections of about 7 µm thickness were cut, deparaffinized, and sequentially stained for CD34 and CD141 using mAbs QBend10 (no. DLN-09135; Dianova, Hamburg, Germany) and TM 1009 (no. M 0617; DAKO, Hamburg, Germany). The staining results with both antibodies were identical in cryo- and paraffin sections. Antigen retrieval was not necessary and even detrimental for both antibodies. In some experiments, QBend10 was used only for single staining.

Single Staining for CD34

The sections were preincubated in glucose/glucose oxidase solution and incubated with QBend10 at a 1:1500 dilution in PBS/BSA/NaN3 with 0.003 mg/ml avidin overnight. Subsequently, the Vectastain ABC Elite kit (no. PK-6102; Vector Labs, Burlingame, CA, distributed by Alexis, Grünberg, Germany) was used according to the manufacturer's instructions with 0.02 mg/ml biotin in the dilution of the secondary biotinylated anti-mouse IgG. Finally, horseradish peroxidase (HRP) was revealed by diaminbenzidine, and the sections were dehydrated and coverslipped in Eukitt.

Subtractive Double-Immunoenzymatic Brightfield Staining

Briefly, MAb QBend10 was diluted 1:1.500 in PBS containing 1% BSA and 0.1% NaN3 and applied overnight at 4C. After washing, the Ultra Vision LP Alkaline Phosphatase (AP) two-step system (no. TL-015-AF; Lab Vision, Fremont, CA, distributed by Medac, Wedel, Germany) was used, applying the ready-to-use "primary antibody enhancer" for 20 min at room temperature and subsequently the prediluted AP polymer for 30 min at room temperature. After washing with Tris-HCL (pH 8.2), AP activity was revealed in dark blue by a Fast Blue reaction for 15 min under protection from light with addition of levamisole. After washing with PBS, TM 1009 was diluted 1:500 and incubated overnight at 4C. Subsequently, the two components of the Ultravision system were applied again, and after washing with Tris-HCl, the Fuchsin$^+$ substrate kit (no. K 0625; DAKO) was used according to the manufacturer's instructions to reveal AP reactivity in red. Incubation with Fuchsin$^+$ lasted for 3 to 5 min at room temperature. Finally, formol pigment was removed by incubating the sections for 5 min at room temperature in 1% ammonia in 70% ethanol. The sections were coverslipped in glycerol gelatine and sealed with acrylate-based mounting medium. Control sections omitting the first or the second primary antibody revealed that the second application of the detection system did not substantially alter the blue color obtained in the first incubation step.

Additive Double-Immunofluorescence Staining

Serial paraffin sections were preincubated in glucose/glucoseoxidase solution as described previously (Steiniger et al. 2005). CD34 was detected by rabbit mAb EP373Y (no. 2150-1, Epitomics, Burlingame, distributed by Biomol, Hamburg, Germany, no. 94643/1) diluted 1:500 in PBS/BSA/NaN3 with 0.003 mg/ml avidin and applied overnight at 4C. After washing, HRP-conjugated anti-rabbit IgG with 0.02 mg/ml biotin and the ABC complex of the Vectastain

Elite Kit (no. BA-1000; Vector Labs, distributed by Alexis) were used according to the manufacturer's instructions. The sections were then incubated with tyramide-conjugated Alexa 488 fluorochrome from TSA kit no. 2 (no. T 20912; Molecular Probes/Invitrogen, Karlsruhe, Germany) diluted 1:100 in amplification buffer with 0.0015% H_2O_2 as indicated by the manufacturer for 10 min at room temperature protected from light. After washing, TM 1009 was diluted 1:50 as described above and applied overnight at 4C, followed by HRP-conjugated anti-mouse IgG and the ABC complex of the Vectastain Elite Kit (no. PK-6102; Vector Labs, distributed by Alexis). Finally, tyramide-conjugated Alexa 555 fluorochrome (TSA kit no. 41, diluted as described above) was applied for 10 min at room temperature. The sections were dehydrated, coverslipped in Eukitt, and stored at room temperature.

Three-Dimensional Reconstruction of Vessels

Image Acquisition, Segmentation, and Transformation. Selected parts of red pulp tissue were photographed with an Olympus E330 digital camera (Olympus, Center Valley, PA) adapted to a Zeiss Axiophot microscope (Carl Zeiss AG, Oberkochen, Germany) using the ×20 lens in the case of brightfield microscopy. This configuration yielded 3136 × 2352 pixels per original image corresponding to 850 × 638 µm. For fluorescence microscopy, an Olympus AX 70 microscope with a ×10 lens and an RT Slider Camera (Diagnostic Instruments, Inc., Sterling Heights, MI) were used, yielding 1600 × 1200 pixels per original image corresponding to 1120 × 840 µm. Serial color images were obtained in a roughly aligned manner using larger structures such as vessels and trabeculae for orientation.

Processing of the images was performed by Python scripts using tools from VTK (visualization toolkit) and Pygame for joystick input handling. All procedures were thus strictly based on license-free open-source software.

A random portion of the splenic red pulp was chosen for investigation. The images were first segmented to sample colored areas. In detail, the red, green, and blue (RGB) images were first transformed into the HSV (hue saturation value) color model and thresholded to exclude color information outside vessels and to separate the two different colors. An alpha channel was introduced, and its values were set transparent in non-colored areas. Thus, red, green, blue, and alpha (RGBA) images with transparent background were obtained. Identical structures were superimposed in two adjacent high-resolution images by two-dimensional translation, by scaling such as extension and compression and by rotation. Display and transformation were accomplished in real time by the OpenGL programming interface and joystick input for convenient operation. Thus, distortions caused by the production and processing of the serial sections were abolished.

The values of the different parameters mentioned above were stored for each image of the series after transformation. From these data, the largest rectangle was computed, which was present in all images. Finally, the images were cropped to eliminate non-overlapping areas. On average, this resulted in the loss of 10% of the image area.

Surface Rendering. The aligned and cropped pixel data of the sections were loaded into a voxel data set. The dimensions of these voxels were anisotropic and depended on image resolution and section thickness. The xy resolution of the images was limited by the optical system and was much below 1 µm, whereas the axial (z) resolution was determined by the assumed average section thickness of 7 µm. To remedy this, the data were resampled and transformed into isotropic voxels of 1 to 2 µm by reducing xy resolution and increasing z resolution by interpolation. The data were processed in three dimensions by application of a closing filter, a Gauss and a median filter, and finally an erosion filter.

Following these manipulations, a 3-D surface model was produced by using the marching cubes algorithm from VTK followed by application of a connection filter to exclude objects with less than 2500 faces of the triangular surface mesh in brightfield and 1.500 faces in fluorescence images.

The model was rendered using an OpenGL graphics card. The ends of microvessels were detected by turning the model on three axes, arbitrarily choosing a point on the surface of an end and highlighting all faces surrounding this point within 15 µm in red. The cut surfaces of the model were visualized in a different color corresponding to the angle of illumination to improve the 3-D effect. In addition, a safety margin to the cut surface, which was excluded from searching for capillaries, was color-coded. The criteria for picking vessel ends were the isolated position of the structures together with a non-complex elongated form and a length of more than 20 µm.

In two of the brightfield and two of the fluorescence specimens, either a small part of the white pulp or a trabecula was included. This area was also eliminated from the reconstructed model (Supplemental Table S1). As capturing small parts of white pulp surface could not be avoided at the magnification used, the volume investigated was different in each section series. The number of sections also differed between 14 and 30 in the individual series (Supplemental Table S1).

Verification of Microvascular Ends

The coordinates of the central point used for highlighting the selected capillary end were retrieved. Its z coordinate value divided by seven (the average section thickness in µm) indicated the section number to be used for verification. Then its xy coordinates were inversely transformed into the coordinates of a point in this section. A small area surrounding the point was cut and saved. The same area

was also retrieved from three sections above and below the point of interest to obtain a small series of seven sections containing the selected capillary end in the central section. Thus, each vessel end highlighted in the model was individually inspected to confirm its isolation from the surrounding sinuses and from other vessels. The number of verified microvascular ends was counted in each series and the mean number of ends per µl was calculated.

Three-Dimensional Visualization of Microvascular Ends with Surrounding Sinuses

To visualize sinuses, an area of 100 µm edge length around the respective end was isolated from the seven aligned images and converted to the HSV color space to extract the staining of the sinuses. The extracted voxel data were smoothened by application of the Gauss filter from VTK and subjected to volume rendering. Finally, the identical volume was retrieved from the capillary surface model. The volume model of the sinuses and the surface model containing the capillary end were then rendered and displayed by an OpenGL graphics card.

Results

CD34 and CD141 in Human Spleens

Serial paraffin sections derived from the red pulp of three individuals were double stained for CD34 and CD141 and observed by brightfield or fluorescence microscopy. The two different techniques were chosen because double staining using immunoenzymatic methods for brightfield microscopy leads to a predominantly subtractive staining result, whereas immunofluorescence methods permit additive color mixing and thus detection of antigen coexpression.

With both methods, CD34, as detected by mAb QBend10, was primarily found in arteriolar and capillary endothelial cells (Steiniger et al. 2007). The staining did not differ in both cell types. Arterioles were defined by a smooth muscle layer visible by staining with hemalum or anti–smooth muscle alpha actin. Small arterioles and metarterioles could, however, not be unequivocally distinguished from capillaries because antibodies directed against components of smooth muscle cells did not react with these vessels. In addition, a special type of fibroblasts at the surface of splenic trabeculae, under the splenic capsule and in the adventitia of larger vessels, also expressed CD34 (Steiniger et al. 2007). In one individual, a few large white blood cells, which may represent hematopoietic stem cells, inside sinuses were strongly positive (not shown). Sinus endothelia in the vicinity of white pulp follicles and T cell zones were faintly $CD34^+$ (Steiniger et al. 2007).

The majority of the $CD34^+$ vessels represented capillaries located between the sinuses of the red pulp. By careful inspection, single or multiple open ends were visible in some capillaries. In such relatively rare cases, the section longitudinally passed along the lumen of a $CD34^+$ vessel for some distance, revealing an open trumpet- or funnel-shaped structure (Fig. 1a–d). Cross sections of capillaries exhibiting lateral openings were observed more frequently (Fig. 2a–c). Whether these openings belonged to ampullary ends or randomly occurred in the course of the vessel could not be determined. It is unlikely that the capillary endothelial cells continue further without expressing CD34 because hemalum counterstain did not reveal any additional endothelial-like nuclei located in continuity in the same section or in adjacent serial sections. In addition, there were a large number of small dot-like or elongated (Fig. 1b) $CD34^+$ structures in the splenic cords, which were much smaller than endothelial cells. The interpretation of these structures was only possible by viewing serial sections as detailed later (Fig. 3a–n).

As published previously (Steiniger et al. 2007), visualization of aligned serial sections in overlay videos (http://www.staff.uni-marburg.de/~steinigb/SupplementaryVideoMaterial/HCB_2007) had revealed that a large number of red pulp microvessels had ends. However, at that time, the exact relationship of these ends to sinuses could not be established because of the lack of a 3-D reconstruction of the microvasculature.

CD141 was primarily found in sinus endothelia. In addition, the typical fibroblastic reticulum cells of the T cell zones and the follicular periphery of the white pulp were also stained (Steiniger et al. 2007). Immunofluorescence revealed that arterial microvessels bordering the white pulp tended to coexpress CD141 and CD34. This fact was not noticed by brightfield immunohistology because of subtractive staining. Because of the rather complicated structure of the white pulp periphery (Steiniger et al. 2005; Steiniger et al. 2006), we decided to limit our investigation to areas of red pulp excluding perifollicular regions and splenic trabeculae, if possible. A very faint non-endothelial expression of CD141 was also found inside and outside sinuses corresponding to white blood cells.

Venule endothelium exhibited variable and sometimes patchy staining for both antigens. The endothelium in larger vessels was $CD34^+CD141^+$ as reported previously (Steiniger et al. 2007).

Three-Dimensional Model of Red Pulp Microvessels and Detection of Microvascular Ends

Two randomly chosen tissue blocks of about 0.5 cm edge length from each of the three individual spleens were

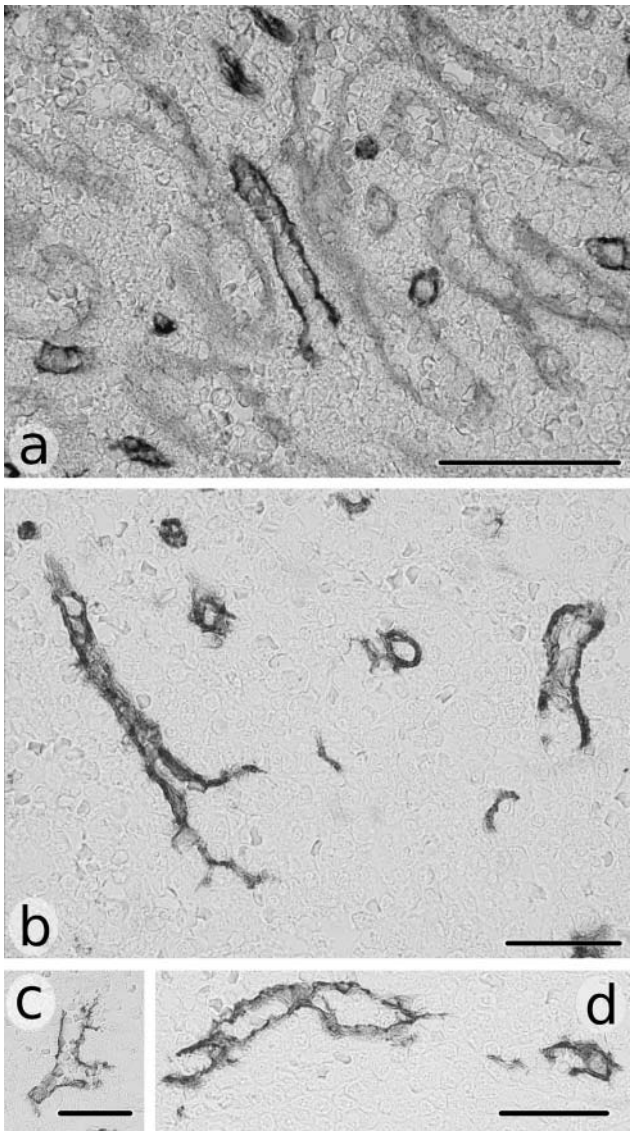

Figure 1. Longitudinal sections of open microvascular (most likely capillary) ends in the splenic red pulp of a 22-year-old man. (a) The endothelium of an open end stained for CD34 (dark) among $CD141^+$ sinuses (light gray). Brightfield double staining. Bar = 50 µm. (b) A large and a small trumpet-shaped end. Note the excessive endothelial branching of the large end. The isolated elongated structures in the right lower part of the image most likely correspond to finger-like final endothelial extensions of additional ends. Single staining for CD34. Bar = 50 µm. (c) Microvessels may exhibit multiple open ends. Single staining for CD34. Bar = 25 µm. (d) Openings in microvessels may also appear as lateral discontinuities of the endothelium. Single staining for CD34. Bar = 50 µm.

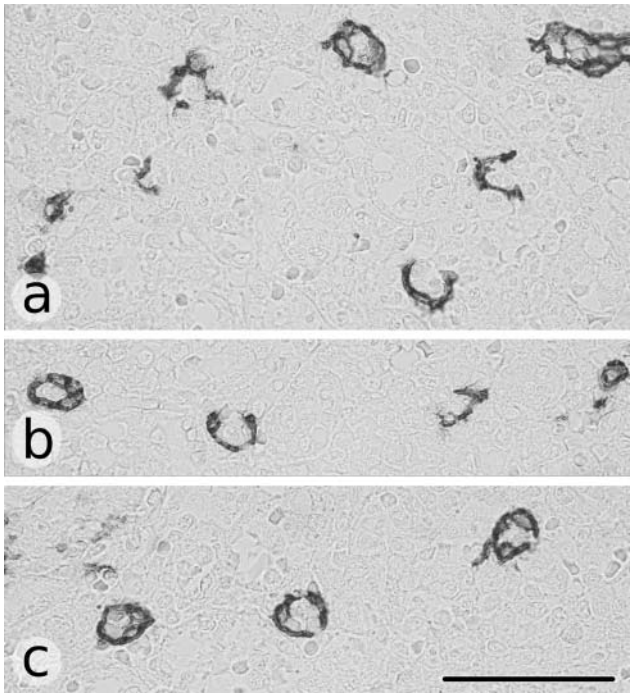

Figure 2. Three different areas (a–c) showing variable types of lateral openings and ends in cross sections of red pulp capillaries (same organ as in Fig. 1). The openings might either be associated with open ends or occur in the entire course of the vessel. Single staining for CD34. Bar = 50 µm.

investigated using brightfield immunohistology and immunofluorescence. Reconstruction of the vasculature was performed from a series of 14 to 30 sections (Supplemental Table S1) double-stained for CD34 and CD141 by using components of the VTK toolkit (Fig. 4a,l and Supplemental Movie S1).

In the process of reconstruction, the volume investigated had to be reduced in comparison to the original tissue block because of three phenomena: First, aligning identical areas in consecutive sections necessitated exclusion of the non-overlapping parts of the photographs. Second, a safety margin of about 14 µm to all cut surfaces was marked and not investigated to avoid incomplete information about the course of microvessels. Third, the white pulp and its surroundings were eliminated from the area of interest because CD34 was weakly expressed in sinus endothelia in this location and because the anti-CD141 (thrombomodulin) reagent also stained fibroblastic reticulum cells. After this procedure, volumes from 0.023 to 0.075 µl (Supplemental Table S1) were used for detecting the ends of arterial microvessels. The ends were highlighted in red after inspection of the model during rotation on different axes and identification of isolated elongated structures longer than 20 µm (Supplemental Movies S2 and S3). To exclude erroneous highlighting, the coordinates of all detected microvascular ends were traced back to the original sections by inverse affine transformation. Three sections above and three sections below the section containing the coordinates of the end were then individually inspected at higher magnification to monitor potential connections to

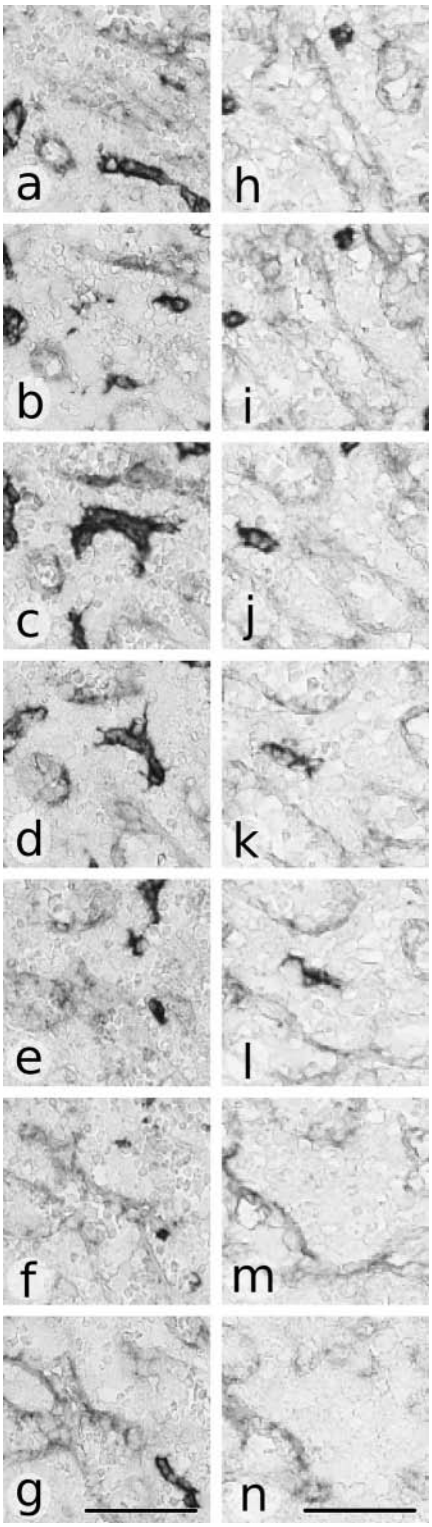

Figure 3. Consecutive serial sections of two different (a–g, h–n) complex capillary ends in the splenic red pulp. Double staining for CD34 (dark microvessels) and CD141 (light gray sinuses). (a–g) Fifteen-year-old male. (h–n) Fifty-year-old woman. The ends are visible in c–e and j–l. The end in c–e exhibits multiple branches with extensions of endothelial cells. Note that these extensions are visible as small dots in b and f. Bar = 50 µm.

sinuses (Fig. 4e–k, p–v and Supplemental Albums S1 and S2) and to verify that the ends were correctly diagnosed. In addition, a 3-D reconstruction of a small volume containing the microvascular end and the surrounding sinuses was produced by combining surface and volume rendering from each series of seven sections (Fig. 4d,o and Supplemental Albums S1 and S2). A detailed analysis of individual ends was necessary because reconstruction of the entire capillary and sinus network of the specimen was not informative as the large sinuses totally shielded the capillaries. Thus, each end was visualized with the help of 11 images (Fig. 4a–v and Supplemental Albums S1 and S2). These images demonstrate the position of the end in the entire two-dimensional section and in the 3-D model, a 3-D magnification of the isolated end from the model, a magnification of the end with surrounding sinuses, and the seven consecutive sections containing the end. After some training, reconstruction of a series of 20 sections with a library of 20 to 30 ends did not take longer than 1 hr.

Human splenic red pulp arterial microvessels formed an anastomosing network in the splenic cords between the sinuses (Fig. 4a,l and Supplemental Movie S1). Most of these vessels were capillaries. In this network, 301 to 888 microvascular ends occurred per µl of the specimen, if the individually verified ends were related to a standard volume (Supplemental Table S1). The minimal total number of ends discovered in all six specimens was 142. A more sophisticated analysis of the data (Supplemental Table S1) was not attempted because of the limited number of individual spleens investigated, the variable volumes and section numbers in each series, the different staining methods, and the unknown location of the investigated specimen in the entire organ.

Endothelial connections between arterial microvessels and sinuses were not detected. The sinuses were also arranged in a network (Fig. 4b,d,m,o), but open funnel-shaped ends were absent. The sinuses drained into larger venules and veins. Connections of arterial microvessels to venules were not encountered.

The seven consecutive sections used for verifying the individual vascular ends also revealed that the endothelial cells forming the end often extended finger-like irregular protrusions (Fig. 3a–n). These structures appeared as small $CD34^{+}$ dots or elongated structures in the individual transverse or longitudinal section, respectively. Thus, serial sections of verified microvascular ends permitted elucidating structures that could not be correctly classified by conventional two-dimensional histology.

Our results show that serial paraffin sections may be reconstructed in three dimensions at an interpolated resolution of about 3.5 µm. The technique permits visualization of vascular structures by combining microscopic and mesoscopic imaging dimensions without necessitating special equipment.

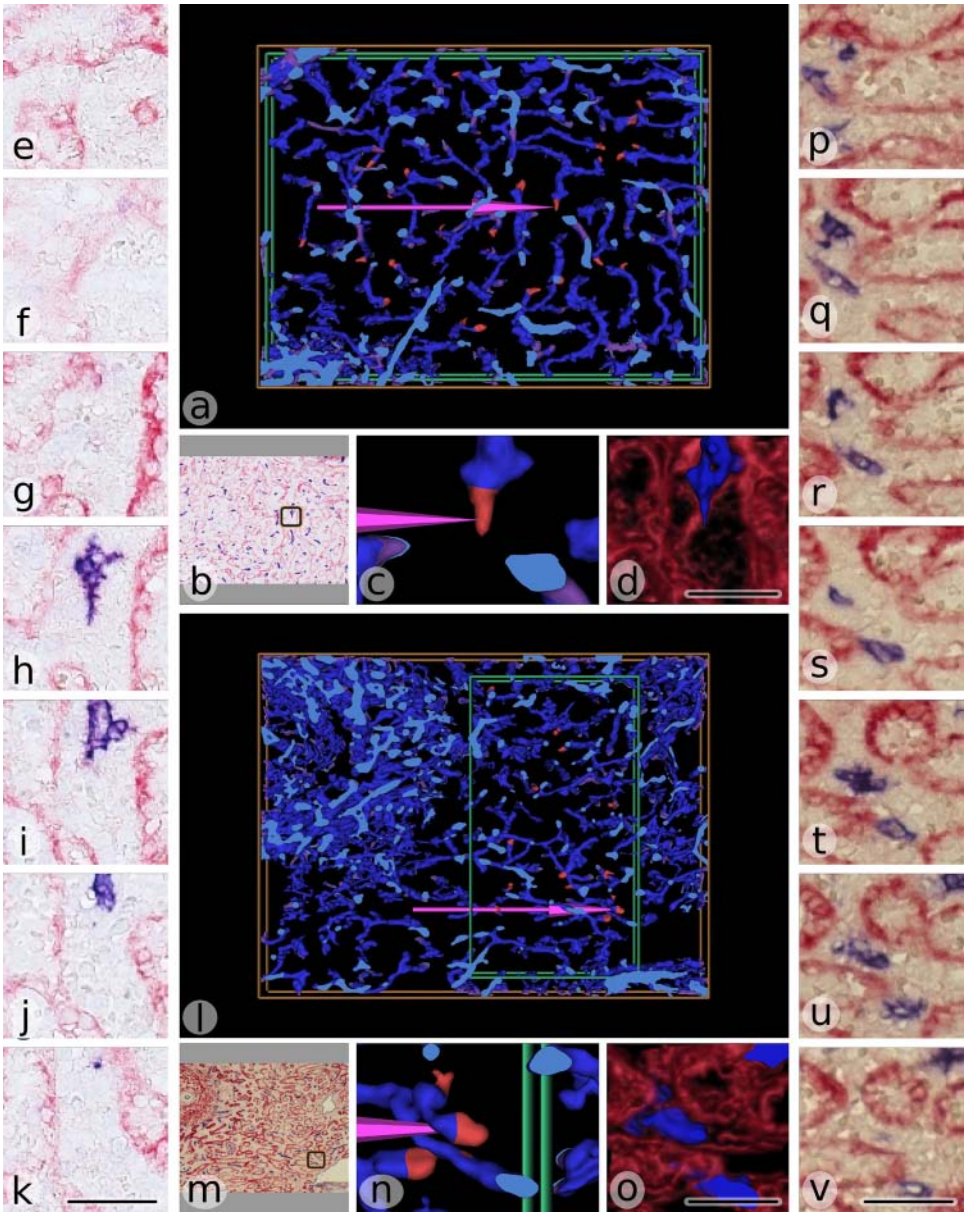

Figure 4. Three-dimensional reconstructions derived from double-stained serial spleen sections of two individuals. (a–k) Spleen specimen 5 (50-year-old woman) and (l–v) spleen specimen 1 (22-year-old man). (a) Three-dimensional surface model of $CD34^+$ microvessels (blue) in a 0.034-µl portion of the splenic red pulp using a series of 20 sections double-stained for brightfield microscopy (see also Supplemental Movie S1). Verified microvascular ends are marked in red. The pink arrow indicates the end visualized in b–k. The magenta-colored portions of the vessels represent a safety margin excluded from searching ends. The green lines delimit the volume used for evaluation. The lower left corner of the model contains a small area of white pulp surrounded by $CD34^+$ sinuses. This area is, however, not present in the entire model and is thus not excluded. (b) Overview of the two-dimensional section showing location of h. (c) Isolated three-dimensional surface model (see also Supplemental Movie S3) of the end indicated in a. The red-colored portion of the end corresponds to h. The entire end is, however, larger and comprises h–j. (d) Three-dimensional surface model of the end (completely colored blue) combined with volume model of the surrounding $CD141^+$ sinuses (red). (e–k) Verification of the end in seven serial sections. There is no connection of the $CD34^+$ end (blue) to the surrounding $CD141^+$ sinuses (light red). (l) Three-dimensional surface model of a 0.023-µl portion of the splenic red pulp using a series of 15 sections double-stained for brightfield microscopy (see also Supplemental Movie S1). Verified microvascular ends are marked in red. The pink arrow indicates the end visualized in m–v. The left part of the model contains the superficial region of a white pulp follicle surrounded by $CD34^+$ sinuses. The green lines delimit the volume used for evaluation. (m) Overview of the two-dimensional section containing s in the black area. (n) Isolated three-dimensional surface model (see also Supplemental Movie S2) of the end indicated in l. The red-colored portion of the end corresponds to t and u. (o) Three-dimensional surface model of the end combined with volume model of the surrounding $CD141^+$ sinuses (red). As demonstrated in t to v, a sinus crosses over a part of the microvascular end. (p–v) Verification of the end in seven serial sections. There is no connection of the end to the surrounding $CD141^+$ sinuses (red). Length of the pink arrow in a and l = 500 µm. Bars = 50 µm.

Discussion

Our investigation is intended to demonstrate methods for finding whether red pulp arterial microvessels in human spleens are connected to sinuses. We have thus performed a 3-D reconstruction of the splenic red pulp microvasculature from immunostained serial sections. The results show that the splenic cords contain an arterial microvascular net with numerous ends, none of which is connected to the meshwork of the red pulp sinuses. The model permits tracing the 3-D information back to the original sections to verify that $CD34^+$ endothelia in capillaries or small arterioles do not anastomose with the $CD141^+$ endothelia investing the red pulp sinuses. We can exclude that the microvessels continue with $CD34^-$ endothelial cells beyond the ends because endothelial nuclei or other capillary-associated structures were missing in this location. In addition, the capillary ends are often split up into long finger-like endothelial extensions, which do not occur in the normal course of vessels. It is thus very likely that apparent lateral openings of the microvessels and open ends represent the beginning of the open splenic circulation.

The reconstruction of human capillaries immunostained for CD34 has been tried before only in tumors (Gijtenbeek et al. 2005; Gilhuis et al. 2006). Our procedure does, however, differ from these studies in three innovative aspects: free software access, the speed of arriving at multiple 3-D models, and the possibility of verifying the results.

The 3-D reconstruction is exclusively based on the VTK toolkit, a license-free open-source software, and on standard hardware components permitting universal reproduction of our data. The images are segmented and manually aligned in real time using a joystick. The procedure is so easy that it does not take longer than about 1 min to process two images. Finally, the coordinates of points of interest, such as microvessel ends, can be traced back to the original sections by inverting the affine transformations and applying them in reversed order. Inspection of the area near the capillary end in seven serial sections permits discussion of the correct diagnosis and exclusion of connections to the adjacent sinuses in each individual capillary end.

Our method tends to underestimate the number of microvascular ends because short ends were disregarded, and an end was only diagnosed if the preceding part of the microvessel was at least 20 μm long. In addition, not all ends may have been recognizable by viewing the model during and after rotation. If the inspection of the seven serial sections surrounding the capillary end yielded an equivocal diagnosis, the respective end was removed from the library. The number of capillary openings may also be much larger than the number of ends detected because multiple discontinuities may occur in the wall of a final capillary segment, as demonstrated in Figure 2a–c. Loss of material between single serial sections did not pose a problem for finding ends. We calculated that on average, not more than 1 μm of tissue was missing between two sections. As CD34 staining does not discriminate between endothelia in capillaries and arterioles, we cannot exclude that some ends belong to arterioles. Thus, we apply the term *microvessel* to indicate this fact, although the majority of the $CD34^+$ vessels in the red pulp were clearly recognized as capillaries.

Due to limited z-axis resolution, the exact shape of the capillary ends cannot be visualized by our 3-D model. Direct visualization of an end by confocal microscopy does not solve this problem because on average, seven serial sections have to be inspected to correctly recognize a capillary end. This is a z-axis range, which cannot be covered by a single thick section. Thus, a reconstruction of the end from several sections cannot be avoided. The procedures used to derive our model may produce "artificial" bulges that may be mistaken for capillary ends. Such structures are created when finger-like extensions of capillary endothelia branch from the vessel surface. It is thus mandatory that each end is verified by tracing the coordinates back to an original section and inspecting the sections above and below. Verification also eliminates misinterpretation of $CD34^+$ fibroblasts at the surface of trabeculae or in the adventitia of large vessels. Small isolated structures such as $CD34^+$ leukocytes in sinuses and in red pulp cords do not interfere because they are eliminated by the filters applied for surface rendering.

The open splenic circulation is assumed to lead the blood along splenic cord stromal fibroblasts into the sinuses via small slits between the sinus endothelia (Fujita 1974; Fujita et al. 1985; Weiss et al. 1985). The vertebrate spleen is thus the only organ where blood flows in spaces not lined by endothelia or other barrier-forming cells. This unique construction permits the direct contact of blood cells and blood-borne materials to sessile red pulp macrophages and plasma cells and the direct secretion of their products into the blood. In addition, the open cord spaces form a reservoir for platelets and reticulocytes in humans (Du P Heyns et al. 1985) and for mature erythrocytes in certain diving and running animal species.

The question of an open or closed microcirculation in human spleens has been discussed for more than hundred years without having yet been settled. Most of the present textbook representations still rely on the fundamental publication of Weidenreich (1901), who depicted two types of human red pulp capillaries found in 3.5-μm thick sections, one anastomosing with a sinus and the other ending free in a splenic cord. The majority of the subsequent investigators, especially groups using scanning electron microscopy (SEM), primarily detected indications of an open circulation without being able to totally exclude a closed system (Fujita 1974; Irino et al. 1977; Kashimura and Fujita 1987).

Van Krieken et al. (1985) tried a 3-D reconstruction of 35 plastic-embedded conventionally stained sections of

human splenic red pulp and did not observe any connections of capillaries and sinuses. SEM studies of corrosion casts (Schmidt et al. 1988) showed capillary ends and were unable to unequivocally demonstrate a larger number of capillary to sinus anastomoses. Corrosion casts suffer from the problem that the casting material may artificially bridge an open capillary end to a sinus wall, if this end is located close to the sinus. In addition, not all parts of the vasculature may have been filled with casting material. Finally, localizing casting material in the open circulation is error prone if the corrosion technique removes all tissue components needed for orientation. The studies by Fujita (1974), Irino et al. (1977), and Kashimura and Fujita (1987) also failed to demonstrate capillary-to-sinus anastomoses in microdissected conventional SEM preparations of the human red pulp and in corrosion casts with the interesting exception of so-called arteriolar labyrinths mentioned in the latter publication. Snook (1950) summarized older literature demonstrating that human red pulp capillaries may end with "ampullae" without joining sinuses. This corresponds to the finding by Fujita et al. (1985), who described three types of arterial endings in the human red pulp by SEM—namely, a funnel-shaped type, an ampullar (sacculated) type with lateral openings, and a complex type. Weiss et al. (1985) inspected large numbers of single human red pulp sections by transmission electron microscopy and only mentioned capillary ends lying between the sinuses but no connections of capillaries and sinuses.

All these older studies have diagnosed vessels by means of their size or ultrastructure. We extend the findings now by also using immunophenotypic differences between sinus and arteriolar/capillary endothelia. As summarized previously (Steiniger et al. 2007), human splenic sinus endothelia exhibit a unique phenotype expressing antigens such as CD8, the macrophage mannose receptor, or CXCL12. More recent own unpublished studies showed that sinus endothelia are also positive for LYVE-1, VEGFR3, and TIE-2 (CD202b) if cryosections are used. The only antigen in addition to CD34 differentiating positive red pulp capillary from negative sinus endothelia was VEGFR2, which could, however, only be detected in cryosections with the antibodies used (Steiniger, unpublished data). Thus, we did not find any other combination of reagents except mAbs QBend10 (anti-CD34) and TM1009 (anti-CD141; thrombomodulin) applicable for double staining of formalin-fixed paraffin sections. The decisive advantage of these mAbs is that they can both be used without antigen retrieval.

Thrombomodulin appears to be either induced or downmodulated in arterial microvessel endothelia by mediators diffusing from the white or the red pulp, respectively. The same is true for CD34 in sinus endothelia. Distinction of capillaries from sinuses at the surface of follicles and T cell zones is thus difficult by immunofluorescence but not by brightfield subtractive staining. Variable antigen expression in splenic sinus endothelia has also been reported in mice (Balazs et al. 2001).

Finally, it may very well be that the shape of some microvascular ends is not preserved in routine histological specimens. We often observed fine finger- or sheet-like extensions of $CD34^+$ endothelia at these ends. In cross section, these extensions appear as isolated dots or streaks of stained material in the splenic cords. If such fine structures are not tightly fixed to extracellular matrix components in vivo, their position may depend on the capillary blood pressure so that they collapse after cessation of blood circulation or due to immersion fixation. Thus, it cannot be excluded that a number of open capillary ends cannot be detected in sections, although they are functional. Perfusion fixation might circumvent this problem, but this method cannot be applied in the clinical setting of emergency splenectomies or pancreas transplantation.

We assume that all capillary ends observed are open because it is very unlikely that long blind and totally closed ends exist in the microvasculature. In addition, we can demonstrate unequivocal open ends in longitudinal sections of a few capillaries. Most open capillary ends inevitably escape detection in a single 7-µm longitudinal section. If the average capillary diameter amounts to about 5 µm, such a section will always include the entire vascular endothelium, which prevents recognition of the vessel lumen.

The results showing that red pulp arterial microvessels are not connected to sinuses are qualitative. Exact quantification of microvascular ends necessitates investigating more individual specimens, larger series of sections, and more different locations within the organ. Final proof of an entirely open system would necessitate studies of the intact microcirculation in vivo, which is beyond any technique presently applicable to humans.

We cannot exclude that there are specialized regions in the splenic red pulp where anastomoses between capillaries and sinuses exist. In one of the three spleens investigated, we found areas of highly branched capillaries and sinuses, which may correspond to the arterial labyrinth with anastomoses described by Kashimura (1985) in a SEM study. The arrangement of the microvessels in these regions differed conspicuously from the other parts of the red pulp, which had a rather regular distribution of capillaries and veins. As this phenomenon was absent in the other four specimens investigated, we regard it as a consequence of a physiological or pathological event leading to localized formation of new vessels with potential anastomoses.

Our findings only apply to the vasculature of the splenic cords. Inspection of serial sections revealed that numerous open capillary ends also occurred at the periphery of the white pulp—for example, in the perifollicular region outside the marginal zone. There is a pronounced network of especially wide non-sheathed capillaries in this region that are fed by sheathed capillaries approaching the perifollicular region from the surrounding red pulp (Steiniger et al.

2007). This capillary plexus may replace the marginal sinus present in mice and rats but absent in humans (Steiniger et al. 2006). Visualization of the superficial capillary network of the white pulp was not within the scope of the present study.

In summary, our results strongly support a primarily open circulation for splenic red pulp microvessels, if immunohistological double staining and an innovative 3-D reconstruction procedure are used. Up to now, it is totally unknown how nature avoids blood coagulation in this open circulation and which forces drive red cells through the tortuous stromal spaces and the interendothelial slits of the sinus walls. Red pulp fibroblasts need to exhibit an anticoagulatory surface, but this has not been investigated up to now. A more detailed immunohistological analysis of splenic red pulp cords and the 3-D arrangement of their vasculature might thus reveal new organ-specific principles of circulation physiology.

Acknowledgments

We thank A. Seiler and K. Lampp for expert technical assistance. A. Hellinger, formerly in the Department of Visceral, Thoracic and Vascular Surgery, Marburg University Hospital, helped obtain the spleen specimens. E. Weihe, Institute of Anatomy and Cell Biology, University of Marburg, kindly offered the opportunity to use the fluorescence microscope and camera from his department.

Declaration of Conflicting Interests

The author(s) declared no potential conflicts of interest with respect to the authorship and/or publication of this article.

Funding

The author(s) disclosed receipt of the following financial support for the research and/or authorship of this article: This work was funded by grant Ste 360/10-1 of the Deutsche Forschungsgemeinschaft and by the Faculty of Medicine of Marburg University.

References

Balazs M, Horvath G, Grama L, Balogh P. 2001. Phenotypic identification and development of distinct microvascular compartments in the postnatal mouse spleen. Cell Immunol. 212:126–137.

Fujita T. 1974. A scanning electron microscope study of the human spleen. Arch Histol Jpn. 3:187–216.

Fujita T, Kashimura M, Adachi K. 1985. Scanning electron microscopy and terminal circulation. Experientia. 41:167–179.

Gijtenbeek JMM, Wesseling P, Maass C, Burgers L, van der Laak JAWM. 2005. Three-dimensional reconstruction of tumor microvasculature: simultaneous visualization of multiple components in paraffin-embedded tissue. Angiogenesis. 8:297–305.

Gilhuis HJ, van der Laak JAWM, Pomp J, Kappelle AC, Gijtenbeek JMM, Wesseling P. 2006. Three-dimensional (3D) reconstruction and quantitative analysis of the microvasculature in medulloblastoma and ependymoma subtypes. Angiogenesis. 9:201–208.

Du P Heyns A, Badenhorst PN, Lötter MG, Pieters H, Wessels P. 1985. Kinetics and mobilization from the spleen of Indium-111-labeled platelets during platelet apheresis. Transfusion. 25:215–218.

Irino S, Murakami T, Fujita T. 1977. Open circulation in the human spleen: dissection scanning electron microscopy of conductive-stained tissue and observation of resin vascular casts. Arch Histol Jpn. 40:297–304.

Kashimura M. 1985. Labyrinthine structure of arterial terminals in the human spleen, with special reference to "closed circulation": a scanning electron microscope study. Arch Histol Jpn. 48:279–291.

Kashimura M, Fujita T. 1987. A scanning electron microscopy study of human spleen: relationship between the microcirculation and functions. Scanning Microsc. 1:841–851.

Schmidt EE, MacDonald IC, Groom AC. 1988. Microcirculatory pathways in normal human spleen, demonstrated by scanning electron microscopy of corrosion casts. Am J Anat. 181:253–266.

Snook T. 1950. A comparative study of the vascular arrangements in mammalian spleens. Am J Anat. 87:31–77.

Steiniger B, Barth P. 2000. Microanatomy and function of the spleen. Adv Anat Embryol. 151:1–100.

Steiniger B, Timphus EM, Barth PJ. 2006. The splenic marginal zone in humans and rodents: an enigmatic compartment and its inhabitants. Histochem Cell Biol. 126:641–648.

Steiniger B, Stachniss V, Schwarzbach H, Barth PJ. 2007. Phenotypic differences between red pulp capillary and sinusoidal endothelia help localizing the open splenic circulation in humans. Histochem Cell Biol. 128:391–398.

Steiniger B, Timphus EM, Jacob R, Barth PJ. 2005. $CD27^+$ B cells in human lymphatic organs: re-evaluating the splenic marginal zone. Immunology. 116:429–442.

Van Krieken JHJM, Te Velde J, Hermans J, Wervaart K. 1985. The splenic red pulp: a histomorphometrical study in splenectomy specimens embedded in methylmethacrylate. Histopathology. 9:401–416.

Weidenreich F. 1901. Das Gefässsystem der menschlichen Milz. Arch Mikrosk Anat. 58:247–376.

Weiss L, Powell R, Schiffman FJ. 1985. Terminating arterial vessels in red pulp of human spleen: a transmission electron microscopic study. Experientia. 41:233–242.